Determination of Atomic Spacings in HOPG and Investigation of Ar^+ Ion Sputter Feature Oxidation Using Scanning Tunnelling Microscopy

Scanning Tunnelling Microscopy

Head of Class: Dr David Ward [Word Count: 2987]

Abstract

In this work, scanning tunnelling microscopy (STM) has been used to determine the bond length within the basal plane of highly oriented pyrolytic graphite (HOPG) as 1.416 ± 0.003Å. The interplanar distance in HOPG was also estimated to be 3.64 ± 0.05Å. These findings present evidence that STM can measure distances on atomic scales sufficiently to discern the relative sizes of features.

Having established confidence in the STM method, Ar^+ ion sputter feature oxidation was then investigated. The oxidation of these features was found to have an activation energy of 150 ± 6 kJ mol^{-1}, which is lower than has been reported for similar processes, such as hole growth around the sputter sites. Hence, it is thought that the features produced by sputtering contain an additional strain within their structure. A method applying these sputtering and oxidation techniques could be used to finely control HOPG surface roughness at the atomic scale.

1 Introduction

Graphite is a versatile material with uses ranging from pencils and batteries to nuclear reactor cores. As such, it is important to understand its properties and how they can be manipulated. Previous works [3, 5, 9] have investigated the effects of heating and sputtering using Ar^+ ions on highly oriented pyrolytic graphite (HOPG), with a particular focus on the holes formed on heating around sites bombarded by Ar^+ ions.

In this work, scanning tunnelling microscopy (STM) has been used to investigate the effect of heating on the small hillock features produced by sputtering before the previously observed hole formation occurs. It is thought that the ability to control the roughness of the atomic surface in this way could be used to control conductivity of HOPG samples, although further work is needed to investigate this. The atomic resolving power of STM is also investigated to ensure these measurements are reliable, and to estimate both the interplanar spacing and the basal plane bond length in HOPG.

A summary of STM and HOPG defect oxidation theory is presented in §2, followed by method, results and discussion for experiments investigating the oxidation of HOPG defects (§3.1) and determining of the HOPG basal plane bond length (§3.2). Conclusions are then presented at §4.

2 Theory

2.1 STM Imaging of HOPG

STM exploits the tunnelling current between an atomically sharp platinum-iridium tip and the electron density surrounding a conducting material to produce images. The application of electric fields across piezoelectric crystals is then used to precisely move this tip. These piezoelectric motors are however susceptible to temperature variations affecting their calibrated response [7, Fig. 6], so thermal variations must be minimised. A schematic overview of STM operation is presented in Figure 1.

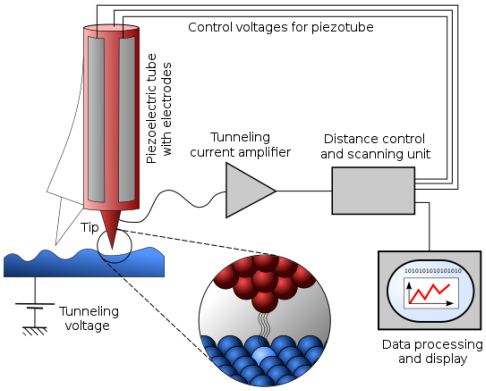

Figure 1: Schematic overview of STM operation [4].

A PID (proportional integral derivative) control loop is used to prevent the tip from colliding with the sample surface. However, this results in over-compensation for sharp features on the surface. This can sometimes results in sharp peaks showing a long trail artifact, referred to as shadowing. The PID control loop can be modified to take measurements in different modes, primarily either one in which the tip height is adjusted to maintain a constant current, or one in which the tip height is kept constant and the tunnelling current recorded. The constant height mode is potentially more useful for surfaces with considerable variation.

The surfaces undergoing analysis are HOPG, which are expected to have the graphite structure presented in Figure 2. This figure also demonstrates how the peaks in electron density measured at atomic scales correspond to where two carbon atoms in the graphite structure are positioned directly above each other, and the dips in electron density to where there is a carbon atom above an empty site in the layer below. Hence, the distances between carbon atoms in each of these layers (basal planes) can be found geometrically as 2/3 times the distance between the electron density peaks.

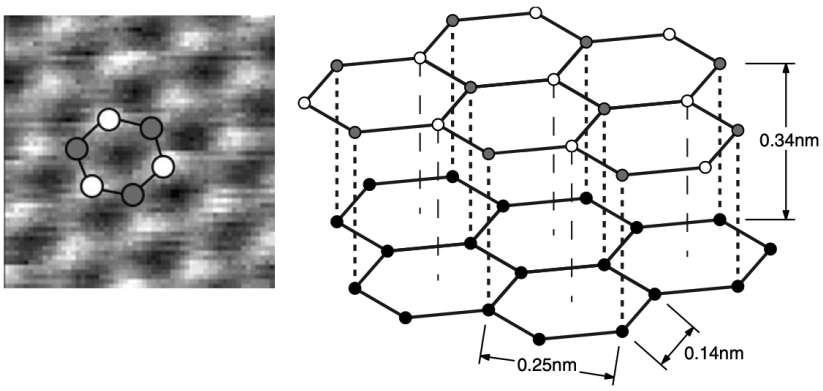

Figure 2: Graphite surface geometry [8, Figure 4-6]. (Left) A measurement with high electron density areas highlighted with white circles, and low electron density areas highlighted with dark circles. (Right) A lattice model of perfect graphite with top layer shading consistent with the left hand image.

2.2 HOPG Defects and their Oxidation

Sputtering a HOPG sample with Ar^+ ions can introduce small hillock features visible to STM observations [9]. Other features which are expected to be visible include steps between atomic layers and holes which form around weakened lattice sites upon sufficient heating [3].

It is hypothesised that upon heating, the size of the Ar^+ hillock features induced by sputtering should decrease, as the violent disruption to the lattice by bombardment introduces additional strains. Hence, it is expected that these features will oxidise before the holes observed in [3] start to form. Assuming that these hillocks are generally of a similar height, then the fraction of the surface which has not been oxidised is proportional to the roughness of the HOPG surface, r. This is defined in equation (1), where $d\Sigma$ represents integration over a sample region of area A, z is the true height of the surface at a given position on the surface, and $\bar{z}$ is the mean height of the surface.

$$r = \frac{\int |z - \bar{z}| \, d\Sigma}{A} \tag{1}$$

The fraction of the surface that has not been oxidised is expected to tend to zero as the heating temperature tends to infinity, and a decrease in roughness is proportional to the rate at which this oxidation occurs. Hence, the roughness measured is expected to follow the modified Arrhenius relationship (2), where E_a is the activation energy for hillock oxidation.

$$r = A \exp\left(\frac{E_a}{k_B T}\right) \tag{2}$$

3 Experiments

3.1 Investigating the Effect of Oxidation on HOPG

3.1.1 Method and Results

Sample Preparation Method

Four samples were used to investigate the oxidation of HOPG. These samples were from the same source, so it will be assumed that each sample has the same properties. These samples were prepared for analysis by following a standard procedure. First, the top layer of the sample was cleaved using sellotape. This was repeated at least twice and until a clean cleave was achieved. The sample was then sputtered using Argon ion bombardment for a time t_{sputt} and at a power P_{sputt}, where both are only relative values. The samples were then heated to temperature T for the chosen time, t_{heat}. This heating process required precise placement of the sample in the centre of the furnace, as it had open ends, resulting in a steep temperature gradient. The process of inserting and removing samples from the furnace therefore introduced a reasonable error in t_{heat}. The heating time was said to begin when the sample reached the centre of the furnace, and the process to remove the sample from the furnace would begin once the desired heating duration had elapsed. Hence, it was found that on average, t_{heat} was (1.5 ± 0.5)s greater than the target time. Finally, to provide conductivity, each sample was attached to a conducting base with evenly spread glue containing silver nanoparticles. This glue was then allowed to dry for 90 minutes, removing measurement distortions induced by the glue shrinking whilst setting.

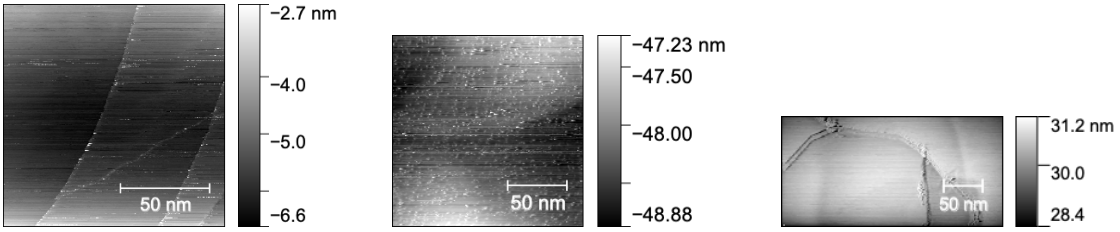

(a) Planar Steps. Observed after sputtering and heating to 760°C for 15s

(b) Sputtering Effect. Observed after sputtering with no heating.

(c) A Hole. Observed after heating an uncleaved sample to 725°C for 15s

Figure 3: Observations of planar step, sputtering and hole features.

Qualitative Observations
Using STM to produce images of sample surfaces between 200nm x 200nm and 500nm x 500nm scales, it is possible to observe large features including: steps between atomic planes, the effects of sputtering, and holes which can form around these sputtered areas, see §2.2, [3, p.10801] and [4, Figure 3]. Steps and sputtering effects were regularly observed, and one hole was imaged. This hole, however, was observed on a fresh sample before it had been cleaved, so its origin is unclear. These observations are depicted in Figure 3.

Previous works [3, 5] which have observed hole formation around etch sites have used heating times on the order of 5-20 minutes, much longer than the 15 to 30 second heating times used here, so the lack of hole observations is expected. The degree of surface roughness, however was seen to change dramatically. The samples depicted in Figure 3b and Figure 3a were both subjected to the same regime during preparation, however the sample in §3a has considerably fewer sputtering features visible, suggesting that the size of features induced via Argon sputtering has been reduced by oxidation, as discussed in §2.2. This effect will be quantified below.

Differences were observed when two images of the same area were produced in direct succession. The atomic step in Figure 4b is significantly more curved than in Figure 4a, and seems to be a function of the STM tip scanning direction (up or down). Therefore, it is difficult to report with any certainty the curvature of steps in the surface. This will be discussed in §3.1.2.

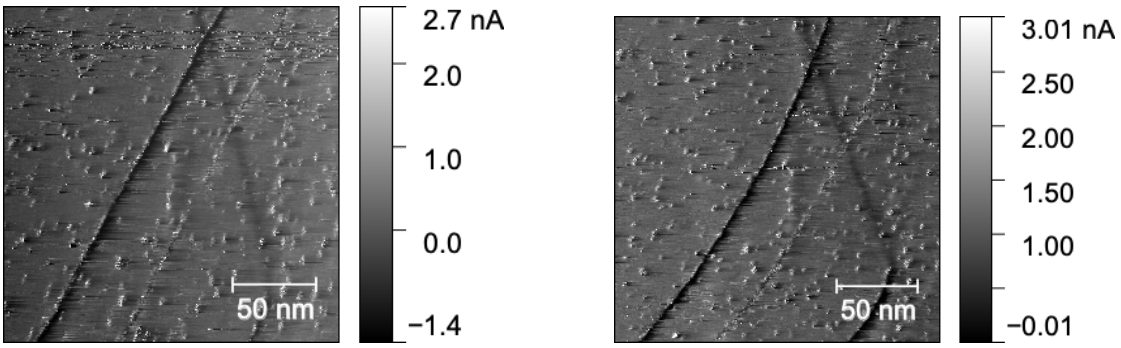

(a) Upward scanning direction

(b) Downward scanning direction

Figure 4: STM images of the same feature demonstrating uncertainty in large scale feature positioning and step curvature.

Surface Roughness Analysis

As noted above, the roughness of sample surfaces induced by sputtering decreases upon heating. To investigate this effect further, samples were prepared using constant conditions: $t_{\text{sputt}} = 0.75$ (relative units), $P_{\text{sputt}} = 2$ (relative units) and $t_{\text{heat}} = 15$s. Each sample was then imaged at a range of temperatures between 670°C and 760°C. The surface roughness of each of these images was then analysed using the process outlined below.

Images were imported into an analysis tool, Gwyddion [6], and images where sputtering features were more visible than the measurement noise were manually identified. Some images had visible sputtering features, but were deemed unusable for quantitative analysis due to large shadowing artifacts. The image would then be cropped to focus on a section of sputtering features across a mostly flat surface. To measure only the average size of the features produced by sputtering, the background of this region would then be further flattened using Gwyddion's inbuilt "Remove polynomial background" feature. This uses a polynomial fitting method where the coefficients $a_{j,k}$ in equation (3)

$$z_{\text{fit}} = \sum_{j=0}^{m} \sum_{k=0}^{n} a_{j,k} x^j y^k \tag{3}$$

are found such as to minimise ΔZ in equation (4). Here, α and β respectively label the x and y indices of the image pixels.

$$\Delta Z = \sum_{\alpha,\beta} \left(z_{\text{fit},(\alpha,\beta)} - z_{\text{measured},(\alpha,\beta)} \right)^2 \tag{4}$$

It was found that by conducting this fitting with $m = n = 5$, the background fluctuations were mostly removed whilst retaining the sputter features themselves. Finally, the surface roughness, r, was calculated using Gwyddion's inbuilt "Statistical Quantities" tool, which determines r using equation (5),

$$r = \frac{\sum_{\alpha,\beta} |z_{\alpha,\beta} - \bar{z}|}{N} \tag{5}$$

where N is the number of pixels analysed. This is a discrete version of (1). This method was preferable to using a root mean square measurement of roughness, as it decreases the weighting given to larger noise-induced peaks.

For each temperature, multiple images were recorded and all suitable images were analysed in the way described above. A total of 80 roughness measurements were recorded. As explained in §2.1, the surface roughness is taken to be proportional to the rate at which the features introduced by sputtering are oxidised. Hence, by (2), average roughness for each temperature was used to plot $\ln r$ against $1/T$ to produce Figure 5. Here, errors have been calculated using $\frac{\sigma}{\sqrt{n}}$ where σ is the sample standard deviation of the

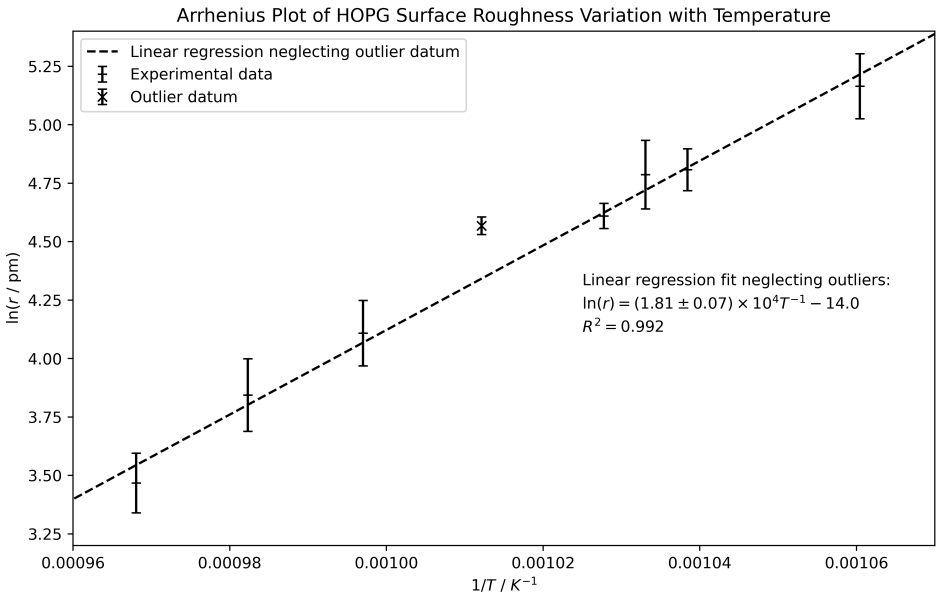

Figure 5: Arrhenius Plot of HOPG Surface Roughness Variation with Temperature.

roughness measurements for that specific temperature, and n is the number of measurements taken at that temperature. Using equation (2) and the best-fit gradient in Figure 5, the activation energy for sputter feature oxidation is found as (150 ± 6) kJ mol^{-1}.

Determination of the HOPG Interplanar Spacing

It was found that images such as that in Figure 3a could be used to estimate the HOPG interplanar spacing by measuring the difference in recorded z positions either side of a step. It was found that some of these steps were two or three atomic layers thick, so this was accounted for in the analysis. In total, 48 steps were analysed, giving an estimate for the interplanar spacing in HOPG of (0.364 ± 0.005)nm.

3.1.2 Discussion - The Effect of Oxidation on HOPG

The observations of steps in the HOPG surface, such as those in Figure 4 reveal a large uncertainty in the curvature and position of measured features. It is thought that this is due to the piezoelectric motors responding differently to motion in the up and down directions. It would be interesting to investigate whether the heating and hence oxidation of HOPG samples results in the straightening of previously curved atomic steps, so further work in this area using a more advanced STM technique would be fruitful. Most of the results presented here are largely statistical in nature, so in this work, these effects are generally negligible.

The outlier datum in Figure 5 was recorded on a sample heated to 715°C. The images produced for this sample were abnormally noisy, possibly due to a poor STM tip being used. This could introduce a systematic increase in the value of $\ln(r)$ for this sample, so this datum has been disregarded in the analysis.

Except for the point marked as an outlier, all of the data presented in Figure 5 fall within one standard deviation of the linear regression fit, giving a value of $R^2 = 0.992$. Hence, it is believed that the effect of oxidation on the features (hillocks) introduced by sputtering is being well represented. The exact mechanism by which this oxidation occurs, however, is unknown and would be well suited for further research. Activation energies for monolayer hole growth in HOPG samples around sputter sites have been reported [3, p.10801] as (168 ± 5) kJ mol^{-1}, which is outside a 2σ range from the activation energy found for this sputter feature oxidation process, (150 ± 6) kJ mol^{-1}. Hence, the features produced by sputtering may have additional strain within their structure, reducing the required energy for bond breaking and hence oxidation. However, further research is required to investigate this in more detail.

Despite the good agreement between results presented in Figure 5, only seven data were used, resulting in relatively high uncertainty for the oxidation process activation energy. The reliability of this analysis could therefore be improved by analysing samples prepared at a greater range of temperatures, and subject to different initial t_{sputt}, t_{heat} and P_{sputt} conditions.

The value for the interplanar spacing in HOPG was determined to be (0.364 ± 0.005)pm. However, this is around 6σ from the values reported in other works [2], which range between 3.336Å and 3.356Å. This overestimation could be explained by the PID controller over-compensating due to the sudden change in atomic height.

3.2 Determination of the HOPG Basal Plane Bond Length

3.2.1 Method and Results

Using STM imaging it is possible to obtain atomic resolution images of a plane of carbon atoms on a HOPG sample, as seen in Figure 6a. As explained in §2.1, these images show the areas of high and low electron density in a HOPG sample and allow for calculation of the carbon-carbon bond length in the graphite basal plane.

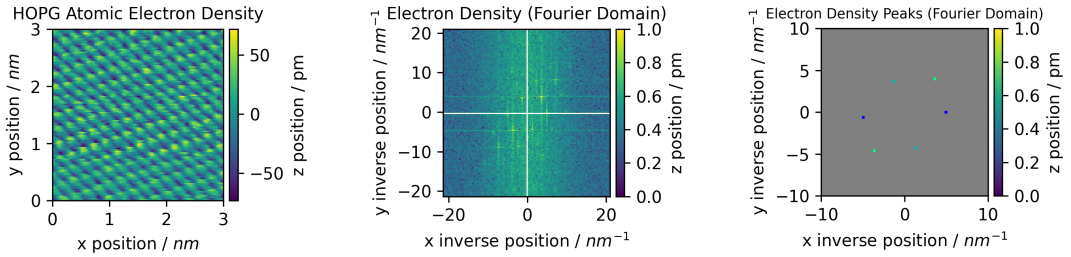

(a) 3nm x 3nm Atomic resolution image of HOPG surface

(b) 2D Fourier transform of (a)

(c) Peaks in (b)

Figure 6: Electron density Fourier transform analysis.

Error Reduction

STM imaging at atomic resolution is extremely sensitive, so precautions were taken to minimise disturbances. These precautions included placing the STM on a vibration isolation table, enclosing the tip area to minimise air movement, allowing the setup to come to thermal equilibrium for around an hour before taking atomic resolution images, and allowing at least 90 minutes for the silver glue attaching samples to the sample holders to dry, as explained in §3.1.1.

The computational method used to analyse these images is composed of two main elements intended to reduce errors. First, a Fourier transform is performed on the image, utilising all of the information in the image to resolve the spatial frequencies at which peaks in electron density occur. This minimises uncertainties but also introduces a quantisation error due to the limited resolution of the images. This quantisation error was minimised by using 3nm x 3nm images of 256 x 256-pixel resolution, as this was found to be the best balance between atomic resolving power and quantisation error reduction. It will be assumed here that these Fourier transforms should produce six primary peaks arranged in a perfect hexagon around the origin, however, this is somewhat disputed [1]. In practice, the peaks form a skewed hexagon (Figure 6c).

The skew seen in the Fourier transform is thought to be due to both: thermal changes affecting the calibration of the piezoelectrics used for positioning, and the fact that the

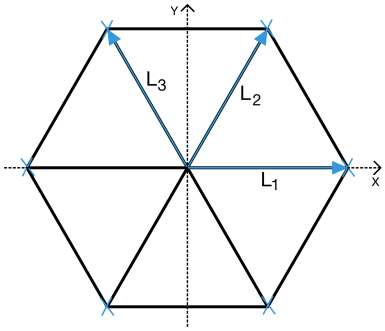

Figure 7: Regular hexagon depicting $\boldsymbol{L_i}$.

STM tip is always at an angle to the surface, introducing angular distortions equivalent to taking the 2D projection of the sample surface in the plane normal to the STM tip. The distortions caused by both of these effects are isomorphic, so the second element of the computation then exploits this isomorphism to remove both distortion-causing effects simultaneously. This is done by finding the 3D rotations which map a regular hexagon of arbitrary side length in the x-y plane to another regular hexagon in 3D space whose projection into the x-y plane matches the inter-peak separations observed.

The Fourier peaks observed are always symmetric about the x-axis, and there are four unknowns in the mapping from distorted hexagon to regular hexagon (side length of the regular hexagon and the three angles to rotate about in 3D). Hence, the most suitable mapping method takes the 2D vector $\boldsymbol{l}_1$ as the reciprocal of the displacement from $P1$ to $P2$ in Figure 6c, and similarly for $\boldsymbol{l}_2$ from $P3$ to $P2$. These can then be considered as the x-y projections of two adjacent vertices of a hexagon which is also distorted into the plane. It is then possible to solve equations (6)

$$\begin{aligned} \boldsymbol{l}_{2,x} &= [R(\alpha,\beta,\gamma)(\boldsymbol{L}_3 - \boldsymbol{L}_2)]_x \\ \boldsymbol{l}_{2,y} &= [R(\alpha,\beta,\gamma)(\boldsymbol{L}_3 - \boldsymbol{L}_2)]_y \\ \boldsymbol{l}_{1,x} &= [R(\alpha,\beta,\gamma)(\boldsymbol{L}_2 - \boldsymbol{L}_1)]_x \\ \boldsymbol{l}_{1,y} &= [R(\alpha,\beta,\gamma)(\boldsymbol{L}_2 - \boldsymbol{L}_1)]_y \end{aligned} \tag{6}$$

where $R(\alpha,\beta,\gamma)$ is the general transformation for rotations by angles α, β and γ about the x, y and z axes respectively and in that order and $\boldsymbol{L}_i$ correspond to vertices of a regular hexagon of side length L_0 as depicted in Figure 7.

$$\begin{aligned} \boldsymbol{L}_1 &= (L_0, 0, 0) \\ \boldsymbol{L}_2 &= (L_0\cos(\pi/3), L_0\sin(\pi/3), 0) \\ \boldsymbol{L}_3 &= (-L_0\cos(\pi/3), L_0\sin(\pi/3), 0) \end{aligned} \tag{7}$$

The value of L_0 then gives a best estimate of the spacing between high electron density peaks observed, which can be converted into basal plane bold length as seen in §2.1.

Results

The process outlined above was undertaken with 43 3nm x 3nm image datasets. Each of these datasets contains four similar copies of the data, one for each combination of when the tip is moving forward or backward, and for current and height measurements. Hence, 172 images were analysed, but where duplicate estimates of the carbon-carbon bond length were recorded for the same overall image dataset, only the first value was retained.

Table 1: Error corrected HOPG basal plane lattice parameter values.

Image Number	Bond Length / Å	Image Number	Bond Length / Å
4892	1.410	4754	1.411
4927	1.400	4768	1.411
4927	1.410	4807	1.362
4894	1.459	4756	1.411
4896	1.459	4780	1.411
4908	1.432	4796	1.411
4748	1.411	4810	1.411
4760	1.411	4800	1.411
4774	1.411	4790	1.459
4788	1.411	4790	1.411
4762	1.411	4784	1.411
4776	1.411	4752	1.411
4772	1.411	4778	1.411
4798	1.411	4786	1.411
4808	1.411	4911	1.395
4942	1.444	4910	1.363
4758	1.411	4904	1.424
4770	1.402	4904	1.432
4943	1.360	4906	1.432
4943	1.432	4898	1.459
4812	1.411	4902	1.432
4806	1.411	4900	1.459
4782	1.411	4914	1.432
4796	1.411		

The 47 results obtained in Table 1 make the Fourier domain quantisation error apparent at the 0.01Å level. However, as the data seems to follow a normal distribution, usual data analysis techniques are most suitable. As such, the mean value for the basal plane carbon-carbon atom spacing is found to be $d_{c-c} = (1.416 \pm 0.003)$Å.

Discussion - Determination of the HOPG Basal Plane Bond Length
The value for d_{c-c} obtained is in agreement between the 1 and 2 σ levels (depending on reference) with theoretical predictions and previous experimental works [2, p.5087], giving confidence in the suitability of the method used. Further work could be undertaken to further decrease errors. For example, by increasing the resolution of images used to further reduce the quantisation error.

The literature [1] suggests some uncertainty in the exact structure of Graphite. Further works could use STM analysis to probe this but would require significant work to reduce the uncertainties in positioning induced by thermal effects on piezoelectric calibration. This could possibly be achieved using an external interferometry-based positioning system.

4 Conclusion

The basal plane carbon-carbon bond length, d_{c-c}, and interplanar spacing, d_i, in HOPG were determined to be $d_{c-c} = (1.416 \pm 0.003)$Å, and $d_i = (3.64 \pm 0.05)$Å respectively. Literature values for d_{c-c} vary between 1.418Å and 1.423Å, and literature values for d_i vary between 3.336Å and 3.356Å [2]. Hence, d_{c-c} is in good agreement with the literature values, but d_i is around 6σ from the accepted result. Therefore, it is believed that STM measurements can provide very accurate atomic length measurements when all sources of error are accounted for, but where this is not possible, such as when determining d_i, only relative scaling can be accurately discerned. The accuracy achievable is thought to be sufficient for the quantitative analysis undertaken in this work.

The surfaces of samples sputtered with Ar^+ ions were seen to decrease in roughness after heating, and the activation energy for this process was found as $E_a = (150 \pm 6)$ kJ mol^{-1}. The activation energy for monolayer hole formation around an etch pit is reported in literature to be (168 ± 5) kJ mol^{-1} [3, p.10801]. These processes may occur by similar mechanisms, so the lower E_a for sputter feature oxidation could be a result of additional strains within the features themselves, however, further work would be required to verify this claim. Nevertheless, the process explored here provides a way to control the small-scale surface roughness of HOPG, and potential applications of this effect should be investigated.

References

[1] Ergun, S. (1973) 'Structure of Graphite', Nature Physical Science, 241(107), pp. 65–67. Available at: https://doi.org/10.1038/physci241065b0.

[2] Lechner, C. et al. (2016) 'First-Principles Study of the Structural, Electronic, Dynamic, and Mechanical Properties of HOPG and Diamond: Influence of Exchange–Correlation Functionals and Dispersion Interactions', The Journal of Physical Chemistry C, 120(9), pp. 5083–5100. Available at: https://doi.org/10.1021/acs.jpcc.5b10396.

[3] Stevens, F., Kolodny, L.A. and Beebe, T.P. (1998) 'Kinetics of Graphite Oxidation: Monolayer and Multilayer Etch Pits in HOPG Studied by STM', The Journal of Physical Chemistry B, 102(52), pp. 10799–10804. Available at: https://doi.org/10.1021/jp982025e.

[4] Wilson, R.J., Allison, W. and Alexandrowicz, G. (Lent term 2024) 'Scanning Tunnelling Microscopy - Oxidation of Graphite: Kinetics on the Atomic Scale', Laboratory manual: Department of Physics, University of Cambridge

[5] Chang, H. and Bard, A.J. (1991) 'Scanning tunneling microscopy studies of carbon-oxygen reactions on highly oriented pyrolytic graphite', Journal of the American Chemical Society, 113(15), pp. 5588–5596. Available at: https://doi.org/10.1021/ja00015a012.

[6] Gwyddion user guide (no date). Available at: http://gwyddion.net/documentation/user-guide-en/ (Accessed: 24 February 2024).

[7] Lu, X., Zhou, S. and Zhao, C. (2014) 'Finite element method analyses of ambient temperature effects on characteristics of piezoelectric motors', Journal of Intelligent Material Systems and Structures, 25(3), pp. 364–377. Available at: https://doi.org/10.1177/1045389X13498309.

[8] nanoSurf (2010) 'Operating Instructions: easyScan 2 STM'. Version 2.2.

[9] Wang, X. et al. (2022) 'The surface defects of HOPG induced by low-energy Ar+ ion irradiation', Applied Surface Science, 585, p. 152680. Available at: https://doi.org/10.1016/j.apsusc.2022.152680.

Acknowledgements

The data for this experiment was collected by a group of four students who each contributed equally to the experimental work.